Smart Structures and Systems, *Vol. 22, No. 4 (2018) 481-493*
DOI: https://doi.org/10.12989/sss.2018.22.4.481

Ultrasonic guided wave approach incorporating SAFE for detecting wire breakage in bridge cable

Pengfei Zhang[1a], Zhifeng Tang[*2], Yuanfeng Duan[3b], Chung Bang Yun[3c] and Fuzai Lv[1d]

[1]*Institute of Advanced Manufacturing Engineering, Zhejiang University, Hangzhou 310027, PR China*
[2]*Institute of Advanced Digital Technologies and Instrumentation, Zhejiang University, Hangzhou 310027, PR China*
[3]*College of Civil Engineering and Architecture, Zhejiang University, Hangzhou 310027, PR China*

(Received April 11, 2018, Revised June 17, 2018, Accepted June 20, 2018)

Abstract. Ultrasonic guided waves have attracted increasing attention for non-destructive testing (NDT) and structural health monitoring (SHM) of bridge cables. They offer advantages like single measurement, wide coverage of acoustical field, and long-range propagation capability. To design defect detection systems, it is essential to understand how guided waves propagate in cables and how to select the optimal excitation frequency and mode. However, certain cable characteristics such as multiple wires, anchorage, and polyethylene (PE) sheath increase the complexity in analyzing the guided wave propagation. In this study, guided wave modes for multi-wire bridge cables are identified by using a semi-analytical finite element (SAFE) technique to obtain relevant dispersion curves. Numerical results indicated that the number of guided wave modes increases, the length of the flat region with a low frequency of L(0,1) mode becomes shorter, and the cutoff frequency for high order longitudinal wave modes becomes lower, as the number of steel wires in a cable increases. These findings were used in design of transducers for defect detection and selection of the optimal wave mode and frequency for subsequent experiments. A magnetostrictive transducer system was used to excite and detect the guided waves. The applicability of the proposed approach for detecting and locating wire breakages was demonstrated for a cable with 37 wires. The present ultrasonic guided wave method has been found to be very responsive to the number of broken wires and is thus capable of detecting defects with varying sizes.

Keywords: ultrasonic guided waves; bridge cables with multi-wires; SAFE; dispersion curves; magnetostrictive transducer; wire breakage detection

1. Introduction

Arch bridges and cable-stayed bridges are widely built today because of their pleasing appearance and ease of construction. The main structural components for these types of bridges are cables. The cables are prefabricated then transported to the construction site for installation. Bridge cables consist of multilayer steel wires arranged in parallel within an equilateral hexagon and with a polyethylene (PE) sheath wrapped around them (see Fig. 1).

The safety of the bridges depends upon the structural integrity of these cables. Vibration based monitoring for cable-supported bridges (Cho *et al.* 2010, Dorvash *et al.* 2014, Jang *et al.* 2010, Kim *et al.* 2010, Wang *et al.* 2016) provides an efficient means for detecting abnormal changes in global behavior such as dynamic deflection and modal properties. However those global features are not sensitive enough to detect local damage, such as wire breakage in cables as in this study. There are many non-destructive testing (NDT) methods such as visual inspection (Shull 2016), radiography (Shull 2016), computed tomography, acoustic emission monitoring (Qin *et al.* 2015), magnetic flux leakage (Makar and Desnoyers 2001, Yim *et al.* 2013) and ultrasound (Shull 2016). However many of the above mentioned NDT methods have limitation in applications to bridge cables. For example, conventional ultrasonic excitation methods including impedance method (Giurgiutiu *et al.* 1999, Huynh and Kim 2016, Min *et al.* 2016, Park *et al.* 2003, Park *et al.* 2007) using bulk waves are impractical for inspecting large or long structural components like cables, because they can only cover a small section of the structure at a time. Guided waves (Rose *et al.* 2004, Rose and Royer 2008, Puthillath and Rose 2010), however, can be used to inspect these kinds of lengthy slender structural components because they only require excitation at a single point, cover a wide acoustical field, and offer long range propagation. The propagation properties of guided waves have been studied for pipes (Zhang *et al.* 2017), overhead transmission lines (Legg *et al.* 2015), ground anchors (Zima and Rucka 2017), rails (Loveday 2012), concrete (Beena *et al.* 2017), and seven-wire steel strands (Treyssède 2016) by a number of researchers. Guided wave-based methods have also been employed in long-term and scalable structural health monitoring (SHM) of structures (Lim *et al.* 2017, Park *et al.*

*Corresponding author, Professor
E-mail: tangzhifeng@zju.edu.cn
[a] Ph.D. Student
E-mail: zhangpengfei@zju.edu.cn
[b] Professor
E-mail: ceyfduan@zju.edu.cn
[c] Professor
E-mail: ycb@zju.edu.cn
[d] Professor
E-mail: lfzlfz@zju.edu.cn

ISSN: 1738-1584 (Print), 1738-1991 (Online)

(a) Bridge cable sample

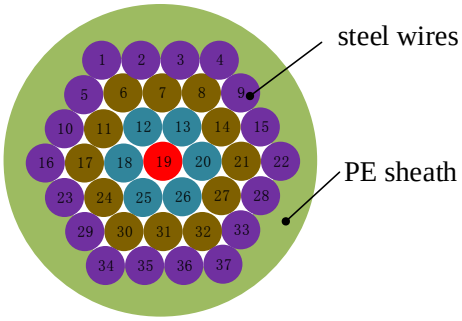

(b) 37 wires cable cross section

Fig. 1 Bridge cable structures

2010, Sohn *et al.* 2014). However, the complex structure of multi-wire cables presents a significant challenge to the application of guided waves for NDT and SHM. It is therefore important to study the properties of guided wave propagation in cables before it is used in such applications.

The mechanical properties of multi-wire cables are more complicated than those of seven-wire strands. The damping and absorption effect of the PE sheath may affect on guided waves in the wires. The most prominent features are the complex geometry of the cross-section and the contact and friction stresses between the wires, which are caused by the processing of hot-extruded PE and the tension load in service. These complex factors constitute the overall mechanical properties of steel wires in bridge cables, which in turn affects how guided waves propagate within them.

In this paper, the effect of complex multi-wire cables on the propagation of guided waves is analyzed. A prerequisite for selection of transducer and design of experimental plan is the provision of guided wave dispersion curves. A semi-analytical finite element (SAFE) (Bartoli *et al.* 2006) method was used to simplify the initial three-dimensional (3D) model into a two-dimensional (2D) model, which was used to calculate dispersion curves and support the subsequent guided wave-based detection of wire breakage. Verification of the SAFE-based dispersion curves was carried out using theoretical results for a single wire and experimental results for a cable with 37 wires.

Experimental study was performed using the L(0,1) mode ultrasonic guided wave in a cable with 37 wires. A magnetostrictive transducer-based guided wave system was used to detect 7 different cases of artificial wire breakages at 3 locations in the cable. The results confirm that the proposed ultrasonic guided wave-based method is very effective for detecting the locations and severities of the wire breakages.

2. Semi-analytical finite element analysis for dispersion curves

2.1 Theory of SAFE

A traditional finite element approach requires Cartesian coordinates to build 3D models for wave propagation analysis in a cable. SAFE approaches (Liu and Achenbach 1994, Bartoli *et al.* 2006, Mu and Rose 2008), by contrast, only require cross-sections in the *x-y* plane to make 2D meshes and build models for these kinds of translationally invariant problem. Using this approach, a 3D guided waves problem can be decomposed into waves with a harmonic exponential solution $e^{i(kz-\omega t)}$ propagating in the longitudinal *(z)* direction. This serves to simplify the propagation model and enhance computing efficiency. The displacement of guided waves can thus be represented as Eq. (1).

$$\vec{\boldsymbol{u}}(x,y,z,t)=\begin{Bmatrix}u_x(x,y,z,t)\\u_y(x,y,z,t)\\u_z(x,y,z,t)\end{Bmatrix}=\begin{Bmatrix}u_x(x,y)\\u_y(x,y)\\u_z(x,y)\end{Bmatrix}e^{i(kz-\omega t)} \quad (1)$$

where, $\vec{\boldsymbol{u}}$ is the displacement vector; $i=\sqrt{-1}$ is an imaginary unit; k is the wave number; $\omega=2\pi f$ is the angular frequency; and t is the time. Using the principle of virtual work, the propagation characteristics of guided waves can be described as follows

$$\begin{gathered}\int_\Gamma \delta\{\vec{\boldsymbol{u}}\}^T\{\vec{\boldsymbol{t}}\}d\Gamma=\\ \int_V \delta\{\vec{\boldsymbol{u}}\}^T\rho\frac{\partial^2\{\vec{\boldsymbol{u}}\}}{\partial t^2}dV+\int_V \delta\{\vec{\boldsymbol{\varepsilon}}\}^T\{\vec{\boldsymbol{\sigma}}\}dV\end{gathered} \quad (2)$$

in which

$$\begin{gathered}\{\vec{\boldsymbol{u}}\}=[\boldsymbol{N}(\xi,\eta)]\{\vec{\boldsymbol{U}}\}e^{i(kz-\omega t)}\\ \{\vec{\boldsymbol{t}}\}=[\boldsymbol{N}(\xi,\eta)]\{\vec{\boldsymbol{T}}\}e^{i(kz-\omega t)}\\ \{\vec{\boldsymbol{\varepsilon}}\}=\left[\boldsymbol{L}_x\frac{\partial}{\partial x}+\boldsymbol{L}_y\frac{\partial}{\partial y}+\boldsymbol{L}_z\frac{\partial}{\partial z}\right]\{\vec{\boldsymbol{u}}\}\\ \{\vec{\boldsymbol{\sigma}}\}=[\boldsymbol{C}]\{\vec{\boldsymbol{\varepsilon}}\}\end{gathered} \quad (3)$$

where, ρ is the mass density; $\delta\{\vec{\boldsymbol{\mu}}\}$ and $\delta\{\vec{\boldsymbol{\varepsilon}}\}$ are the virtual displacement and virtual strain, respectively; $\{\vec{\boldsymbol{U}}\}$ is the nodal displacement vector which is expressed using the shape function matrix $[\boldsymbol{N}(\xi,\eta)]$; ξ and η are the local coordinate for each element, $-1\le\xi\le1$ and $-1\le\eta\le1$; the superscript T denotes the matrix transposition; Γ is the surface of the element; V is its volume; $\{\vec{\boldsymbol{t}}\}$ is the external traction vector which is expressed using $[\boldsymbol{N}]$ and nodal external traction vector $\{\vec{\boldsymbol{T}}\}$; $\{\vec{\boldsymbol{\sigma}}\}$ is the stress vector;

$[\boldsymbol{C}]$ is the material stiffness matrix for each element; and $[\boldsymbol{L}_i]$ are the gather matrices, i.e.

$$\boldsymbol{L}_x=\begin{bmatrix}1&0&0\\0&0&0\\0&0&0\\0&0&0\\0&0&1\\0&1&0\end{bmatrix}\quad \boldsymbol{L}_y=\begin{bmatrix}0&0&0\\0&1&0\\0&0&0\\0&0&1\\0&0&0\\1&0&0\end{bmatrix}\quad \boldsymbol{L}_z=\begin{bmatrix}0&0&0\\0&0&0\\0&0&1\\0&1&0\\1&0&0\\0&0&0\end{bmatrix} \tag{4}$$

By expanding the terms for kinetic energy and strain energy in Eq. (2) and simplifying, the relationship between the external force $\{\vec{\boldsymbol{F}}\}$ and the nodal displacement vector $\{\vec{\boldsymbol{U}}\}$ can be obtained as

$$\{\vec{\boldsymbol{F}}\}=([\boldsymbol{K}_1]+ik[\boldsymbol{K}_2]+k^2[\boldsymbol{K}_3])\{\vec{\boldsymbol{U}}\}-\omega^2[\boldsymbol{M}]\{\vec{\boldsymbol{U}}\} \tag{5}$$

in which the force vector, and stiffness and mass matrices can be obtained as in conventional finite element analysis

$$\begin{aligned}\{\vec{\boldsymbol{F}}\}&=\int_{-1}^{1}\int_{-1}^{1}[\boldsymbol{N}]^T[\boldsymbol{N}]\{\vec{\boldsymbol{T}}\}d\xi d\eta\\ [\boldsymbol{K}_1]&=\int_{-1}^{1}\int_{-1}^{1}[\boldsymbol{B}_1]^T[\boldsymbol{C}][\boldsymbol{B}_1]d\xi d\eta\\ [\boldsymbol{K}_2]&=\int_{-1}^{1}\int_{-1}^{1}([\boldsymbol{B}_1]^T[\boldsymbol{C}][\boldsymbol{B}_2]-[\boldsymbol{B}_2]^T[\boldsymbol{C}][\boldsymbol{B}_1])d\xi d\eta\\ [\boldsymbol{K}_3]&=\int_{-1}^{1}\int_{-1}^{1}[\boldsymbol{B}_2]^T[\boldsymbol{C}][\boldsymbol{B}_2]d\xi d\eta\\ [\boldsymbol{M}]&=\int_{-1}^{1}\int_{-1}^{1}\rho[\boldsymbol{N}]^T[\boldsymbol{N}]d\xi\, d\eta\end{aligned} \tag{6}$$

in which

$$\begin{aligned}[\boldsymbol{B}_1]&=[\boldsymbol{L}_x]\frac{\partial[\boldsymbol{N}]}{\partial x}+[\boldsymbol{L}_y]\frac{\partial[\boldsymbol{N}]}{\partial y}\\ [\boldsymbol{B}_2]&=[\boldsymbol{L}_z][\boldsymbol{N}]\end{aligned} \tag{7}$$

For an unloaded cable ($\{\vec{\boldsymbol{F}}\}=0$), Eq. (5) becomes a generalized eigenvalue problem (Hayashi *et al.* 2003). When the angular frequency ω is specified, we can obtain eigenvalues k and the corresponding eigenvectors, which are the nodal displacements representing the modes of wave propagation. The eigenvalues may be complex, while the real parts correspond to propagating guided wave modes and the imaginary parts correspond to evanescent modes. The relationship between k and ω provides the dispersion curves for the waveguides. For each guided wave mode at ω, the phase velocity can be calculated using $c_p=\omega/k_{RE}$ (here, the subscript *'RE'* means the real part) and the group velocity can be calculated using $c_g=\partial\omega/\partial k$. Thus, the group and phase velocity dispersion curves can be drawn by capturing a range of angular frequency ω. Note that some researchers have used the helical coordinates in SAFE equations to solve the dispersion problems of helical structures (Treyssède 2008), such as cables with twisted wires.

2.2 Dispersion curves using SAFE

Guided waves travel with a different velocity depending on the frequency of the wave. Group velocity dispersion curves are needed to determine the wave propagation speed for each mode. With this information available it is possible to convert the time-of-flight (ToF) into the distance travelled by wave packets in a structure, which is essential for localization of damage. In order to understand dispersion phenomena in cables, SAFE models were established for a variety of different cables with different number of wires (i.e., 7, 19 and 37 wires), while the diameter of each wire is 7 mm.

The case of a single wire can be considered to be the same as a simple rod, whose dispersion properties can be obtained analytically using Pochhammer-Chree equations (Gazis 1959). For a single wire, 3-noded elements are used and the SAFE mesh is shown in Fig. 2(a). The detailed parameters here are as follows: wire radius R=3.5 mm, elasticity modulus E=210e9 Pa, Poisson's ratio ν=0.29, and density ρ=7800 kg/m^3. For verification of the present SAFE-based dispersion curves, the results are compared with those by Pochhammer-Chree equations in Fig. 3, which shows good agreement between two results, especially in the low frequency range.

However, it is difficult to establish analytically the Pochhammer-Chree equations for multi-wire cables because of their complex geometry and contact between individual wires. This is why we chose to use the SAFE method to analyze the dispersion curves. By using the SAFE, we were able to arrive at a simplified multi-wire cable model. The contact condition between wires was assumed to be rigid, making the structure approximate to a rod (Hayashi *et al.* 2003). The cross-section of the cable was meshed using COMSOL (Nucera 2012), shown in Fig. 2. The FE mesh size was taken to be smaller than 1/20 (Kirby 2008) of the wavelength corresponding to the wave frequency of 200 kHz. The guided wave modes with frequencies below 200 kHz were analyzed for 3 different cables (with 7, 19 and 37 wires). The results for dispersion curves are shown in Figs. 4(a)-4(c), from which it can be found that as the number of wires increases, the number of branching modes for a mode family increases as well, making the dispersion relationship more complicated.

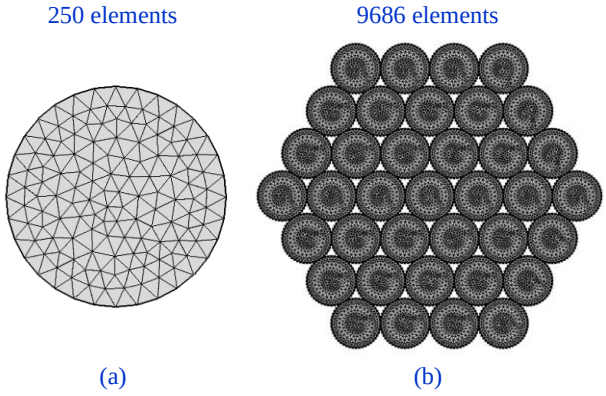

Fig. 2 Cross section meshes of cables for SAFE analysis: (a) with 1 wire and (b) with 37 wires

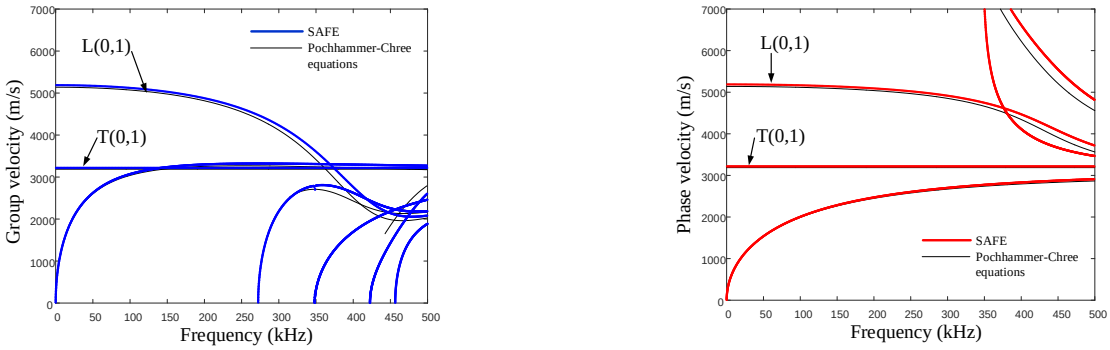

Fig. 3 Dispersion curves for a single wire obtained by Pochhammer-Chree equations and SAFE

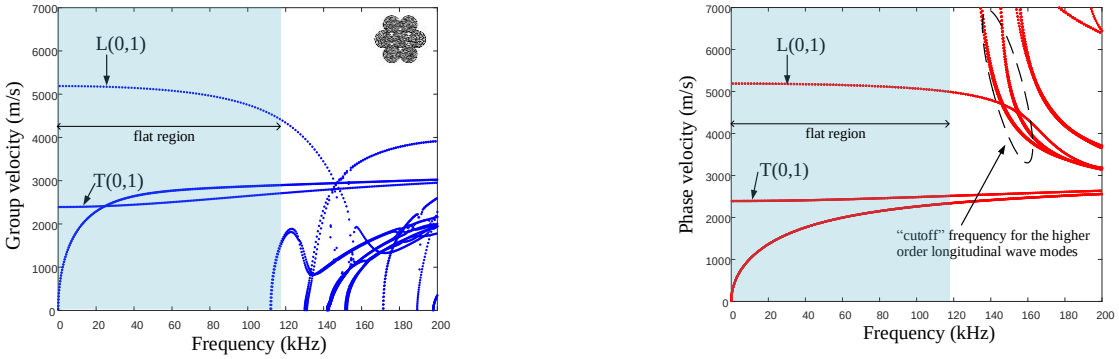

(a) Cable with 7 wires

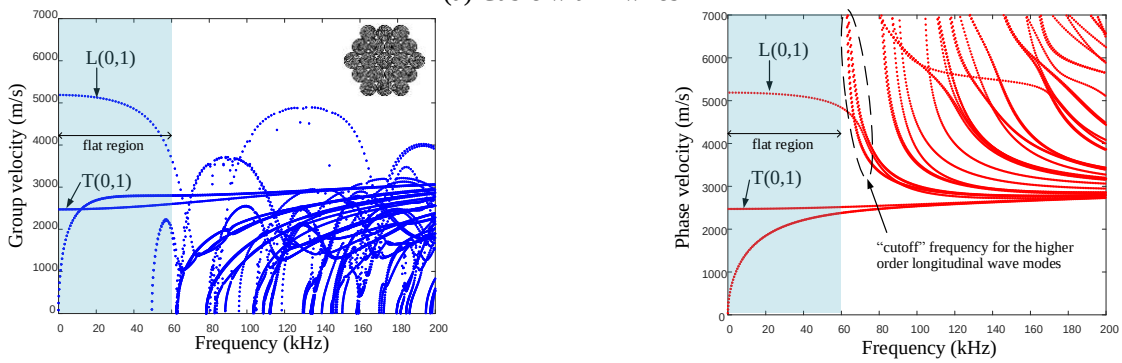

(b) Cable with 19 wires

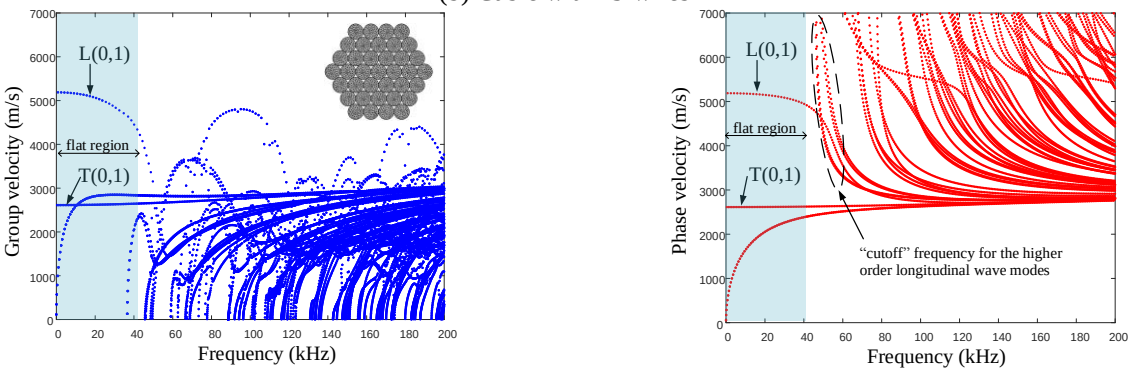

(c) Cable with 37 wires

Fig. 4 Dispersion curves for cables with different numbers of wires using SAFE

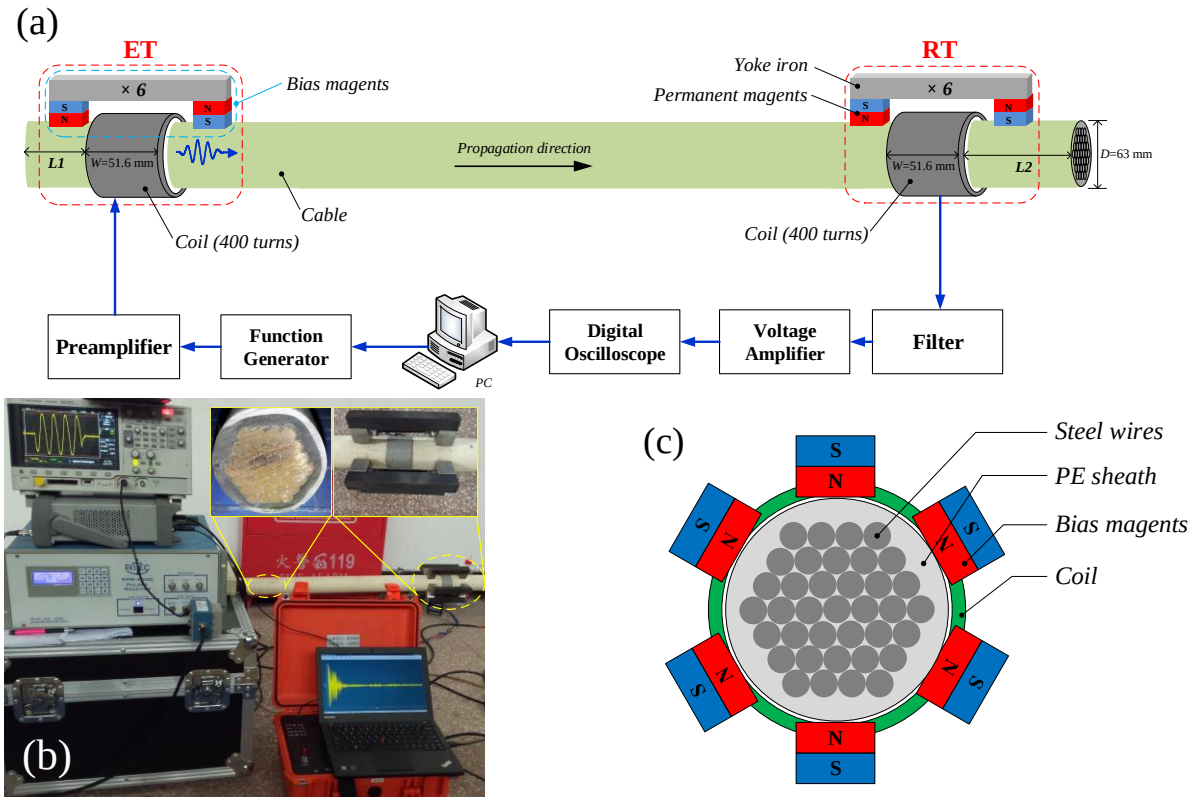

Fig. 5 Experimental set-up for defect detection in a cable using guided waves: (a) Schematic of experiment, (b) Photo of experiment system and (c) Magnetostrictive transducer for longitudinal guided wave

Guided wave modes in a cylindrical waveguide are composed of the longitudinal and torsional waves (Ditri and Rose 1992) *L(m,n)* and *T(m,n)*, where $m \in \{0,1,2,...\}$ denotes the circumferential order and $n \in \{1,2,3,...\}$ stands for the *nth* root of the characteristic equation. All of the curves are dispersive in nature and indicate group and phase velocities are functions of frequency, although certain sections of curves are flatter and less dispersive than the others, such as in the low frequency range for the low order fundamental longitudinal L(0,1) mode which is the preferred mode for experiments.

The most noticeable feature in the group and phase velocity dispersion curves is that as the number of wires increases, the length of the flat region for the lower frequency of the L(0,1) modes becomes shorter and the cutoff frequency for the higher order longitudinal wave modes becomes lower. This means that for cables with many wires, it is difficult to choose a less dispersive frequency range and the measured guided wave signal is more difficult to analyze.

3. Experimental validation

3.1 Experimental set-up

A cross-section view of the cable considered in this experimental study is depicted in Fig. 1(c). The cable is comprised of 37 steel wires, which are arranged in parallel in four layers. The exterior of the wire bundle is surrounded by a 7 mm thick hot-extruded PE sheath. The diameter of each individual wire is 7 mm. The diameter of the entire cable is 63 mm, with a length of 5 m.

A magnetostrictive (Jiles 1995) guided wave experimental inspection system was employed, as shown in Fig. 5. Guided waves were actuated in the cable through magnetic excitation. This causes mechanical strain in the steel wires through the magnetostrictive effect that is known as Joule effect. Conversely, for detection, the inverse magnetostrictive effect that is known as Villari effect enables guided waves to be detected through modifications in the magnetic induction (Kim and Kwon 2015, Bartels *et al.* 1996). The guided waves were generated in the experiment through a dynamic magnetic field (provided by a 51.6 mm wide encircling coil with 400 turns) being superimposed upon a static magnetic field (provided by six permanent bias magnets), thereby enhancing the excitation and detection of the waves. The role of the bias magnets is to provide a static magnetic field that is consistent with the direction of the dynamic magnetic field and to overcome the Frequency-doubling Effect of ferromagnetic materials (Kim and Kwon 2015). These two parallel magnetic fields will cause the steel wires in the cable to alternately expand and contract based on the magnetostrictive effect, and thereby longitudinal guided waves are created.

For each bias magnet configuration, the components include two Ne-Fe-B N50 permanent magnets of size 30×40×30 mm^3, and a yoke iron of size 30×120×25 mm^3.

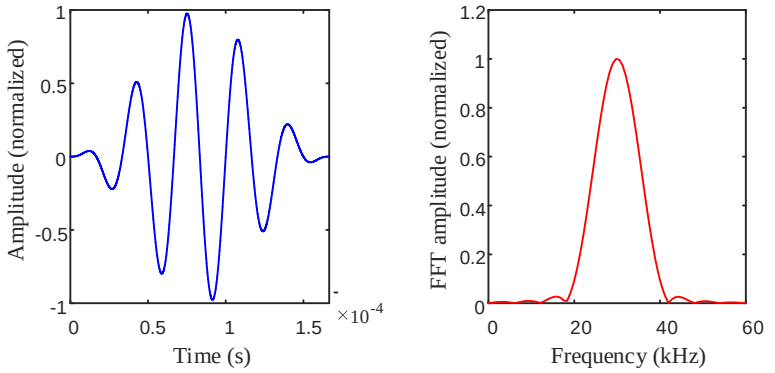

Fig. 6 Excitation signal: Hann-windowed 5-cycle sinusoidal tone burst

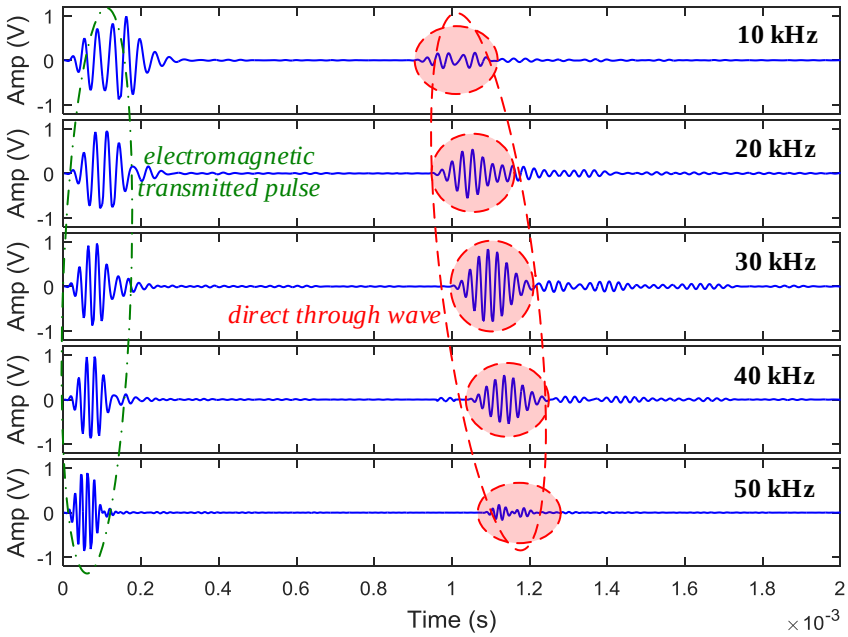

Fig. 7 Signals at RT for different excitation frequencies: a cable with 37 wires

The coils consist of a plastic sheathing to conveniently install on the cable, 10 layers (40 turns per layer) of 16AWG enamel-coated magnetic wire. The coils and 6 bias magnets made up both the excitation transducer (ET) and the detection transducer (RT) (see Fig. 5(c)). These were used to excite and receive longitudinal L(0,1) mode guided waves with center frequencies of 10 kHz, 20 kHz, 30 kHz, 40 kHz and 50 kHz. The structures of the ET and the RT are the same, as both of them can actuate and receive guided waves. For actuation, the ET coil was driven by a PC-controlled current preamplifier (Ritec4000) with a Hann-windowed 5-cycle sinusoidal tone burst (see Fig. 6). On the other hand, the detected voltage signal in the RT coil was bandpass filtered and amplified by about 60 dB. The positions of the two transducers on the cable can be flexibly adjusted. *L1* is the distance between the left end of the cable and the ET. *L2* is the distance between the RT and the right end of the cable.

In this study two methods were used to inspect structures using guided waves: pitch-catch and pulse-echo. Pitch-catch inspection was used to analyze the dispersion and attenuation characteristics of guided waves, without considering the effects of anomaly reflection: with ET as a transmitter and RT as a receiver. Pulse-echo inspection was used to detect anomaly locations (e.g., defects) and their severity. The pulse-echo technique uses only one transducer, an ERT, as the transmitter and receiver simultaneously.

3.2 Validation of dispersion properties

In order to verify the accuracy of the dispersion curves obtained using SAFE for the multi-wire cables, a series of experiments were carried out. The low-order longitudinal mode L(0,1) was selected for the experiments. The excitation transducer ET and the receiving transducer RT were placed close to the left and right ends of the 5-meter-

Table 1 Comparison of group velocities for L(0,1)

Freq.	SAFE group velocity (m/s)	ToF of the second packet (ms)	Experimental velocity (m/s)	Error (%)
10 kHz	5200	0.927	5394	3.59%
20 kHz	5050	0.951	5258	3.95%
30 kHz	4800	1.013	4936	2.75%
40 kHz	4100	1.065	4695	12.67%
50 kHz	3300	1.142	4378	24.63%

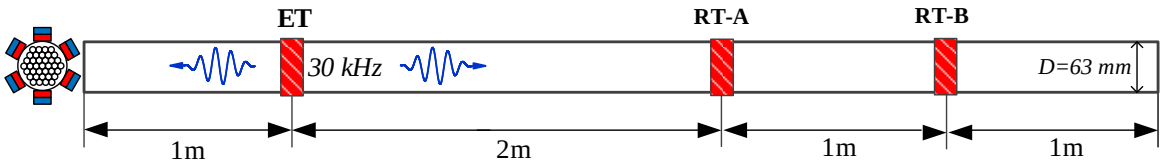

Fig. 8 Schematic of pitch-catch detection experiment

long cable, respectively (*L1≈0, L2≈0*). The signals were received by the RT are shown in Fig. 7.

In Fig. 7, the exciting frequencies of the signals from top to bottom are 10 kHz, 20 kHz, 30 kHz, 40 kHz and 50 kHz. The first portion of the waveform is the electromagnetic transmitted pulse coupled directly from the ET to the RT. The second wave packet marked by a circle in each signal is the direct through wave excited by the ET. It can be seen from the figure that the second packets delay as the excitation frequency increases. This means that the group velocity decreases with an increase in frequency in the L(0,1) mode. As a result of the significant aggravation of the dispersion at 50 kHz (Fig. 4(c)), the amplitude of the 50 kHz direct through-wave signal is so attenuated that it is difficult to distinguish. The above results show how guided waves with different frequencies interact with the waveguide. It has been found that the amplitudes of the direct through waves become largest with an exciting frequency of 30 kHz. Therefore 30 kHz was determined to be the optimal excitation frequency for subsequent experiments.

In guided wave propagation, the group velocity determines how long it will take for guided waves to travel through a specimen. By simply measuring the time-of-flight (ToF) for different reflections of the signal, the group velocity can be determined. The signals in Fig. 7 were analyzed in detail in order to assess the accuracy in the SAFE dispersion curves. For each excitation frequency, the experimental group velocity in mode L(0,1) was calculated using the ToF of the second wave packet of the waveform (direct through wave). The distance between the ET and the RT was 5 m. We can get the group velocity value by dividing the distance by the ToF. The group velocity values for the different frequencies calculated by SAFE (Fig. 4(c)) and the experiments are compared in Table 1.

Table 1 shows that two sets of group velocities by SAFE analysis and experiments match very well for low frequencies (10, 20, 30 kHz) with error less than 4%. However the error increase as the exciting frequency increases. This suggests that it is practicable to use SAFE to analyze dispersion characteristics at low frequencies. However, for more accurate SAFE models for high frequencies, the contact stress between the wires and other potential influencing factors need to be considered.

3.3 Pitch-catch detection for wave travel distance

The above experiments have shown that the L(0,1) mode, which has better dispersion properties in the lower frequency range, is best suited to detecting defects. In another experiment that used the same setup as above, the excitation transducer ET was installed 1 m away from the left end of the cable (*L1=1 m*) and two receiving transducers, RT-A and RT-B, were installed at positions 3 m and 4 m away from the left end, respectively ($L2_A$*=2 m*, $L2_B$*=1 m*). A schematic showing the locations of the transducers along with the experimental setup is presented in Fig. 8. The plots in Figs. 9-10 show the waveforms received by RT-A and RT-B. In Figs. 9(b) and 9(c), the horizontal axis is the wave travel distance converted from the wave travel time using the wave group velocity for the L(0,1) mode which was obtained experimentally as 4936 m/s as in Table 1. For more accurate estimation of the wave travel distance, Hilbert transformation was used, while time-frequency transformation (short time Fourier transformation: STFT) was used for effective examination of the frequency characteristics of the received signals.

The first portion of the received signal is the initial electromagnetic pulse. The other wave packets with high peaks are corresponding to the reflected waves from two ends of the cable with various wave travel paths as summarized in Fig. 11. The amplitudes of the RT-A signals decrease as the wave travel distance increases. This is due to the attenuation causing by the multi-wire structure and the PE sheath. The strongest frequency component in the time-frequency spectra is found as 30 kHz as in Fig. 9(c) and Fig. 10(c), which is consistent with the excitation frequency at the ET.

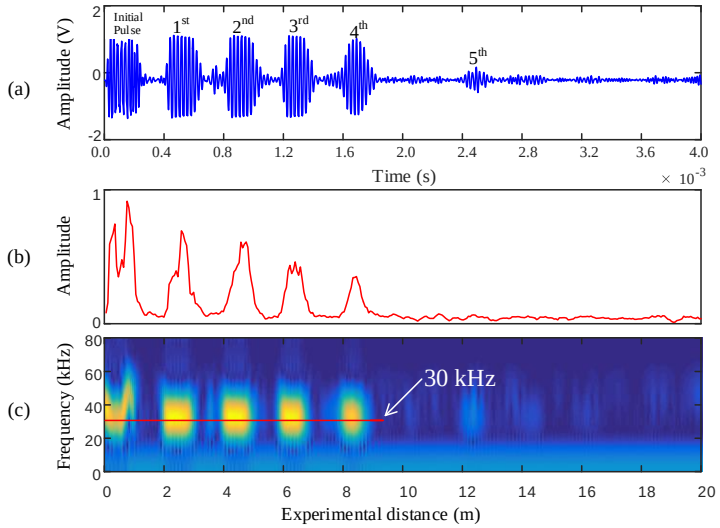

Fig. 9 Signals obtained at RT-A: (a) Time domain signal, (b) Hilbert envelope signal and (c) Time-frequency analysis spectrum

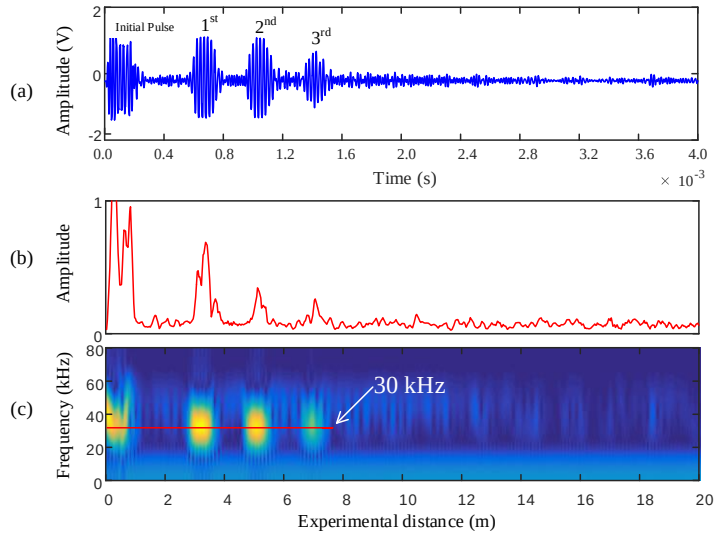

Fig. 10 Signals obtained at RT-B: (a) Time domain signal, (b) Hilbert envelope signal and (c) Time-frequency analysis spectrum

Table 2 Estimated wave travel distances for RT-A

Wave Packet No.	1st	2nd	3rd	4th	5th
Exact distance (m)	2	4	6	8	12
ToF (ms)	0.41	0.82	1.21	1.63	2.45
Estimated distance (m)	2.02	4.05	5.97	8.05	12.09
Error (%)	1.2	1.2	0.5	0.6	0.8

Table 3 Estimated wave travel distances for RT-B

Wave Packet No.	1st	2nd	3rd
Exact distance (m)	3	5	7
ToF (ms)	0.62	1.05	1.38
Estimated distance (m)	3.06	5.18	6.81
Error (%)	2.0	3.7	2.7

The wave travel distances for five wave packets in the RT-A signals were calculated using Hilbert envelopes and the results are shown in Table 2. It has been found that the estimated wave travel distances are excellent with the errors less than 1.5% for various wave paths. Similar results for RT-B case are shown in Table 3, where errors for the distances of the wave paths are found to be less than 4%.

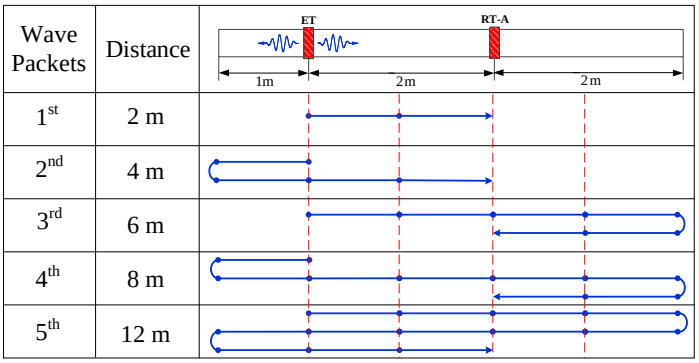

(a)

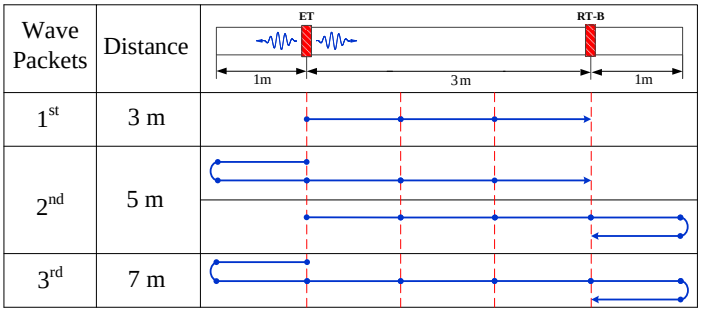

(b)

Fig. 11 Schematic of the guided wave propagation paths: (a) between ET and RT-A and (b) between ET and RT-B

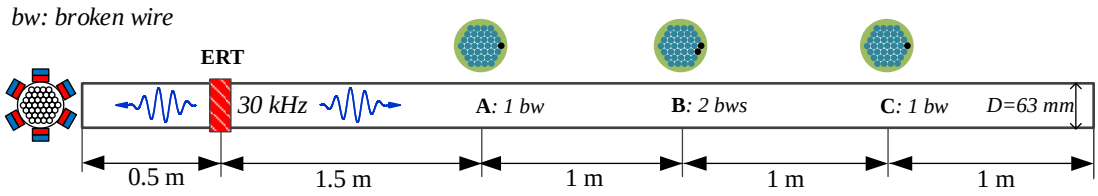

Fig. 12 Schematic of pulse-echo defect detection experiment

4. Guided wave-based wire breakage detection

4.1 Detection and localization of wire breakage

In order to investigate the applicability of guided waves to detect defects in a cable, the same cable with 37-wires utilized in Section 3 was used, but with artificial defects at 3 locations as shown in Fig. 12. Defect 1 was with one broken wire at Position A: 2 m away from the left end. Defect 2 was with two broken wires at Position B: 3 m away from the left end. Defect 3 was with one broken wire at Position C: 4 m away from the left end.

In order to make artificial defects, we used a saw to carefully peel off a small section (3-5 cm) of PE sheath at the location where the defects need to be made until the wire bundle was completely exposed. Such a small removal of the PE sheath has no effect on the test results for wire breakage. PE is a type of acoustical impedance material to the guided wave, therefore, it is the main factor affecting the detection distance of wire damage in the cable using guided wave.

The pulse-echo method was employed by using a single transducer, ERT, for both exciting and receiving the guided waves. The ERT was installed 0.5 m away from the left end ($L1$=0.5 m, $L2$=4.5 m). This method is better suited to actual on-site testing because only one transducer needs to be installed on a cable near the bridge deck. The exciting frequency of the transducer was taken to be 30 kHz. The signal received at ERT is shown along with the Hilbert envelope and the time-frequency transformation in Fig. 13. Wave packets in Fig. 13 represent different paths of reflected waves from the defects and ends of the cable as described in Table 4. The second, third, and fourth wave packets in Fig. 13 and Table 4 correspond to the reflected waves from the defects at A, B, and C, respectively. Table 4 also shows the ToFs and peak amplitudes of the wave packets. The guided wave acoustical distance for each wave packet was calculated and compared with the exact travel distance. The experimental wave velocity of 4936 m/s in Table 1 was used to calculate the experimental wave travel distance. The results are summarized in Table 4, which shows that the estimated wave travel distances for 6 cases of wave packets are very good: with error less than 6%.

Table 4 Estimated wave travel distances for the ERT

Wave Packet No.	1st	2nd	3rd	4th	5th	6th
Exact distance (m)	1	3	5	7	9	10
ToF (ms)	0.21	0.63	1.04	1.50	1.89	2.07
Estimated distance (m)	1.037	3.110	5.133	7.404	9.329	10.218
Amp. (V)	1.90	1.00	0.81	0.36	1.80	0.52
Error (%)	3.66	3.66	2.67	5.77	3.66	2.18
Paths of reflected wave	T→LE→T	T→**A**→T	T→**B**→T	T→**C**→T	T→RE→T	T→RE→LE→T

T: ERT transducer
LE: left end
RE: right end
***A**: artificial damage A (1 broken wire)*
***B**: artificial damage B (2 broken wires)*
***C**: artificial damage C (1 broken wire)*

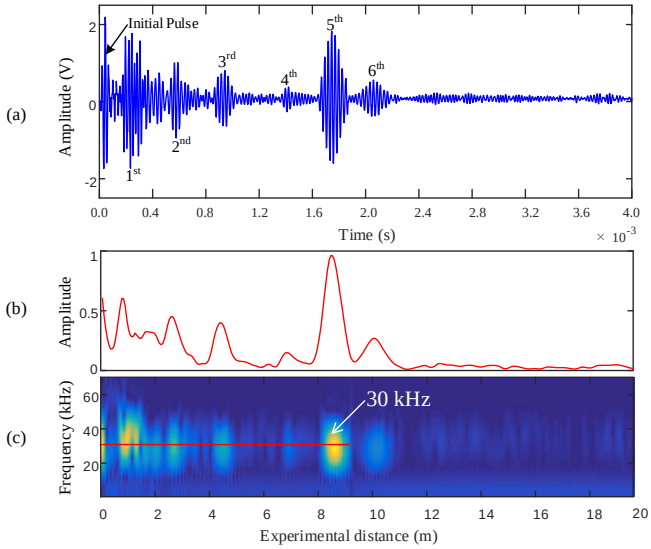

Fig. 13 Signals obtained at ERT: (a) Time domain signal, (b) Hilbert envelope signal and (c) Time-frequency analysis spectrum

4.2 On breakage severity

In order to demonstrate the applicability of the present guided wave method to detect multiple broken wires in the cable, additional experiments were carried out on the same cable with increasing numbers of broken wires at Locations A, B, and C. Each stage of broken wires is summarized as:

Stage I: Same as the case in Section 4-1 (1, 2, and 1 broken wires at A, B, and C).
Stage Ⅱ: Stage I and Increase of broken wires at B to 5.
Stage Ⅲ: Stage Ⅱ and Increase of broken wires at C to 5.
Stage Ⅳ: Stage Ⅲ and Increase of broken wires at C to 10.
Stage Ⅴ: Stage Ⅳ and Increase of broken wires at B to 10.
Stage Ⅵ: Stage Ⅴ and Increase of broken wires at A to 5.
Stage Ⅶ: Stage Ⅵ and Increase of broken wires at A to 10.

The received signals at 7 stages are shown in Fig. 14, which show that the locations of the wave packets corresponding to the positions of the broken wires remain the same. Peak amplitudes of the wave packets for various damage stages are summarized in Fig. 15. As the number of broken wires increased, the amplitudes of the wave packets reflected at the locations of broken wires increased significantly. Such trends are more apparent for the defects at locations (A and B) near the transducer (see Fig. 15), as in the later part of the curve for the 2nd wave packet representing the wire-breakage at A and the first part for the 3rd wave packet corresponding to the wire-breakage at B. This demonstrates that the present ultrasonic guided wave-based system is very responsive to the size of the defect and is capable of detecting the severity of the wire breakage.

5. Conclusions

In this study at first SAFE analysis was carried out for wave dispersion analysis of ultrasonic guided waves in multi-wire cables, then experimental study was performed for validation of the SAFE-based dispersion curves and detection and localization of wire breakages using guided waves. The main findings are summarized below:

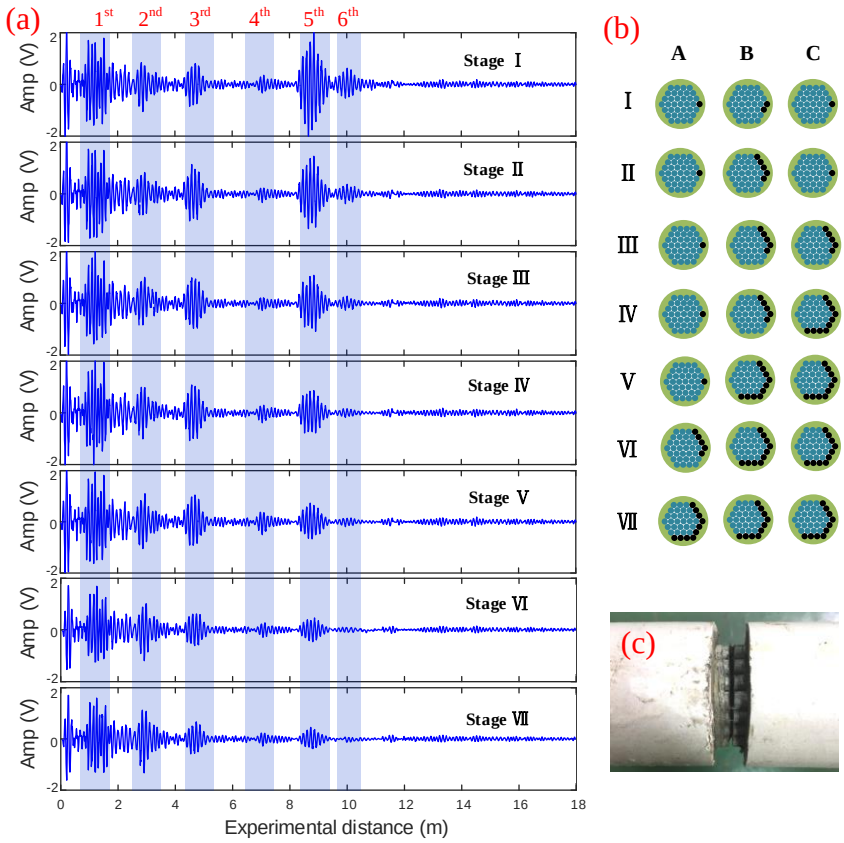

Fig. 14 Signals obtained at ERT for various stages of artificial defects: (a) Time domain signals, (b) Schematic drawing of broken wires at 3 locations and (c) Representative photograph of artificial defect of broken wires

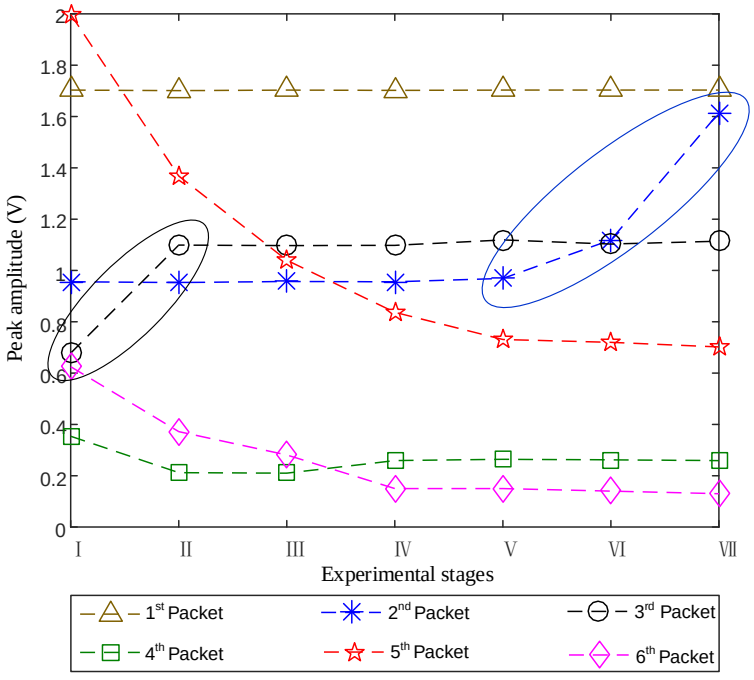

Fig. 15 Peak amplitudes of the reflected wave packets at various damage stages

1. The SAFE-based dispersion curves for a single wire cable are found to be excellent in comparison with the analytical results obtained by Pochhammer-Chree equations. SAFE analysis on the cables with multi-wires shows that the length of the flat region with low frequency for L(0,1) mode becomes shorter and the cutoff frequency for higher order longitudinal modes becomes lower as the number of wires increases. Accordingly, lower excitation frequencies need to be considered for detection of defects in multi-wire cables.

2. SAFE-based group velocities for L(0,1) mode at low frequencies (10, 20, and 30 kHz) are found to be in excellent agreement with the experimental results with error less than 4%. The optimal exciting frequency was selected as 30 kHz for a cable with 37 wires in the subsequent experiments for defect detection.

3. Experimental study using a magnetostrictive transducer system in a pulse-echo configuration indicates that the localization accuracy for 3 artificial defects of wire breakage was very good with error less than 6%. It is also found that the present method is very responsive to the size of the defect (i.e., the number of broken wires), particularly for the defects near the transducer.

As to future research, it is suggested to refine the SAFE model to include the contact and friction stresses among the wires and to carry out experimental study further for different types of defect such as wire corrosion.

Acknowledgments

The authors acknowledge the supports from the Natural Science Foundation of China (No. 61271084, No. U1709216) and the Science and Technique Plans of Zhejiang Province (No. 2017C01042).

References

Bartels, K.A., Kwun, H. and Hanley, J.J. (1996), "Magnetostrictive sensors for the characterization of corrosion in rebars and prestressing strands", *Nondestruct. Eval. Bridge. Highways*, **2946**, 40-50.

Bartoli, I., Marzani, A., Lanza Di Scalea, F. and Viola, E. (2006), "Modeling wave propagation in damped waveguides of arbitrary Cross-Section", *J. Sound Vib*., **295**(3), 685-707.

Beena, K., Shruti, S., Sandeep, S. and Naveen, K. (2017), "Monitoring degradation in concrete filled steel tubular sections using guided waves", *Smart Struct. Syst.*, **19**(4), 371-382.

Cho, S., Jo, H., Jang, S., Park, J., Jung, H., Yun, C., Spencer Jr, B.F. and Seo, J. (2010), "Structural health monitoring of a cable-stayed bridge using wireless smart sensor technology: data analyses", *Smart Struct. Syst.*, **6**(5-6), 461-480.

Ditri, J.J. and Rose, J.L. (1992), "Excitation of guided elastic wave modes in hollow cylinders by applied surface tractions", *J. Appl. Phys.*, **72**(7), 2589-2597.

Dorvash, S., Pakzad, S.N. and LaCrosse, E.L. (2014), "Statistics based localized damage detection using vibration response", *Smart Struct. Syst.*, **14**(2), 85-104.

Gazis, D.C. (1959), "Three-dimensional investigation of the propagation of waves in hollow circular cylinders. I. Analytical foundation", *J. Acoust. Soc. Am.*, **31**(5), 568-573.

Giurgiutiu, V., Reynolds, A. and Rogers, C.A. (1999), "Experimental investigation of E/M impedance health monitoring for spot-welded structural joints", *J. Intel. Mat. Syst. Str.*, **10**(10), 802-812.

Hayashi, T., Song, W.J. and Rose, J.L. (2003), "Guided wave dispersion curves for a bar with an arbitrary Cross-Section, a rod and rail example", *Ultrasonics*, **41**(3), 175-83.

Huynh, T. and Kim, J. (2016), "Compensation of temperature effect on impedance responses of PZT interface for prestress-loss monitoring in PSC girders", *Smart Struct. Syst.*, **17**(6), 881-901.

Jang, S., Jo, H., Cho, S., Mechitov, K., Rice, J.A., Sim, S., Jung, H., Yun, C., Spencer Jr., B.F. and Agha, G. (2010), "Structural health monitoring of a cable-stayed bridge using smart sensor technology: Deployment and evaluation", *Smart Struct. Syst.*, **6**(5-6), 439-459.

Jiles, D.C. (1995), "Theory of the magnetomechanical effect", *J. Phys. D: Appl. Phys.*, **28**(8), 1537.

Kim, J., Swartz, A., Lynch, J.P., Lee, J. and Lee, C. (2010), "Rapid-to-deploy reconfigurable wireless structural monitoring systems using extended-range wireless sensors", *Smart Struct. Syst.*, **6**(5-6), 505-524.

Kim, Y.Y. and Kwon, Y.E. (2015), "Review of magnetostrictive patch transducers and applications in ultrasonic nondestructive testing of waveguides", *Ultrasonics*, **62**, 3-19.

Kirby, R. (2008), "Modeling sound propagation in acoustic waveguides using a hybrid numerical method", *J. Acoust. Soc. Am.*, **124**(4), 1930-1940.

Legg, M., Yücel, M.K., Kappatos, V., Selcuk, C. and Gan, T. (2015), "Increased range of ultrasonic guided wave testing of overhead transmission line cables using dispersion compensation", *Ultrasonics*, **62**, 35-45.

Lim, H.J., Kim, Y., Sohn, H., Jeon, I. and Liu, P. (2017), "Reliability improvement of nonlinear ultrasonic modulation based fatigue crack detection using feature-level data fusion", *Smart Structu. Syst.*, **20**(6), 683-696.

Liu, G.R. and Achenbach, J.D. (1994), "A strip element method for stress analysis of anisotropic linearly elastic solids", *J. Appl. Mech.*, **61**(2), 270-277.

Loveday, P.W. (2012), "Guided wave inspection and monitoring of railway track", *J. Nondestruct. Eval.*, **31**(4), 303-309.

Makar, J., and Desnoyers, R. (2001), "Magnetic field techniques for the inspection of steel under concrete cover", *NDT & E Int.*, **34**(7), 445-456.

Min, J., Yun, C. and Hong, J. (2016), "An electromechanical impedance-based method for tensile force estimation and damage diagnosis of post-tensioning systems", *Smart Struct. Syst.*, **17**(1), 107-122.

Mu, J. and Rose, J.L. (2008), "Guided wave propagation and mode differentiation in hollow cylinders with viscoelastic coatings", *J. Acoust. Soc. Am.*, **124**(2), 866-874.

Nucera, C. (2012), "Propagation of nonlinear waves in waveguides and application to nondestructive stress measurement", Ph.D. Dissertation, University of California, San Diego, United States.

Park, G., Sohn, H., Farrar, C.R. and Inman, D.J. (2003), "Overview of piezoelectric impedance-based health monitoring and path forward", *Shock Vib. Digest*, **35**(6), 451-464.

Park, H., Sohn, H., Yun, C., Chung, J. and Kwon, I. (2010), "A wireless guided wave excitation technique based on laser and optoelectronics", *Smart Struct. Syst.*, **6**(5-6), 749-765.

Park, S., Grisso, B.L., Inman, D.J. and Yun, C. (2007), "MFC-based structural health monitoring using a miniaturized impedance measuring chip for corrosion detection", *Res. Nondestruct. Eval.*, **18**(2), 139-150.

Puthillath, P. and Rose, J.L. (2010), "Aircraft bond repair patch inspection using ultrasonic guided waves", *Review of Progress in Quantitative Nondestructive Evaluation*, San Diego,

California, USA, July,
Qin, L., Ren, H., Dong, B. and Xing, F. (2015), "Development of technique capable of identifying different corrosion stages in reinforced concrete", *Appl. Acoust.*, **94**, 53-56.
Rose, J.L., Avioli, M.J., Mudge, P. and Sanderson, R. (2004), "Guided wave inspection potential of defects in rail", *NDT & E Int.*, **37**(2), 153-161.
Rose, J.L. and Royer, R.L. (2008), "A guided wave health monitoring approach for civil structures", *Proceedings of the 26th IMAC: Conference and Exposition on Structural Dynamics 2008*, Orlando, Florida, USA, February,
Shull, P.J. (2016), *Nondestructive Evaluation: Theory, Techniques, and Applications*, CRC press, Boca Raton, Florida, USA.
Sohn, H., Lim, H.J., DeSimio, M.P., Brown, K. and Derriso, M. (2014), "Nonlinear ultrasonic wave modulation for online fatigue crack detection", *J. Sound Vib.*, **333**(5), 1473-1484.
Treyssède, F. (2008), "Elastic waves in helical waveguides", *Wave Motion*, **45**(4), 457-470.
Treyssède, F. (2016), "Dispersion curve veering of longitudinal guided waves propagating inside prestressed Seven-Wire strands", *J. Sound Vib.*, **367**, 56-68.
Wang, H., Tao, T., Li, A. and Zhang, Y. (2016), "Structural health monitoring system for Sutong Cable-stayed Bridge", *Smart Struct. Syst.*, **18**(2), 317-334.
Yim, J., Wang, M.L., Shin, S.W., Yun, C., Jung, H., Kim, J. and Eem, S. (2013), "Field application of elasto-magnetic stress sensors for monitoring of cable tension force in cable-stayed bridges", *Smart Struct. Syst.*, **12**(3-4), 465-482.
Zhang, X., Tang, Z., Lv, F. and Yang, K. (2017), "Scattering of torsional flexural guided waves from circular holes and Crack-Like defects in hollow cylinders", *NDT & E Int.*, **89**(7), 56-66.
Zima, B. and Rucka, M. (2017), "Non-Destructive inspection of ground anchors using guided wave propagation", *Int. J. Rock Mech. Min. Sci.*, **94**, 90-102.

HJ